Nuclear Engineering and Technology 54 (2022) 2253–2261

Contents lists available at ScienceDirect

Nuclear Engineering and Technology

journal homepage: www.elsevier.com/locate/net

Original Article

Enhancement and optimization of gamma radiation shielding by doped nano HgO into nanoscale bentonite

Elhassan A. Allam [a, b, *], Rehab M. El-Sharkawy [c], Atef El-Taher [d], E.R. Shaaban [d], RedaElsaman [d], E. El Sayed Massoud [e, f], Mohamed E. Mahmoud [a]

[a] Alexandria University, Faculty of Science, Chemistry Department, P.O. Box 426, Ibrahimia 21321, Alexandria, Egypt
[b] Ministry of Health and Population, Central Labs of Alexandria, P.O. Box 21518, Alexandria, Egypt
[c] Chemistry Department, Faculty of Dentistry, Pharos University in Alexandria, P.O. Box 37, Sidi Gaber, Alexandria, Egypt
[d] Physics Department, Faculty of Science, Al-Azhar University, Assuit Branch, 71524 Assuit, Egypt
[e] Biology Department, Faculty of Sciences and Arts, King Khalid University, P.O. Box 28, 61953, Dahran Aljanoub Saudi Arabia
[f] Research Center for Advanced Materials Science (RCAMS), King Khalid University, Abha, Saudi Arabia

ARTICLE INFO

Article history:
Received 20 June 2021
Received in revised form
31 October 2021
Accepted 20 December 2021
Available online 23 December 2021

Keywords:
Nano-bentonite
Nano-mercuric oxide
Doping process
γ-ray shielding properties

ABSTRACT

In this study, nano-scaled shielding materials were assembled and fabricated by doping different weight percentages of Nano-mercuric oxide (N-HgO) into Nano-Bentonite (N-Bent) based on using (100-x% N-Bent + x% N-HgO, x = 10, 20, 30, and 40 wt %). The fabricated N-HgO/N-Bent nanocomposites were characterized by FT-IR, XRD, and SEM and evaluated to evaluate their shielding properties toward gamma radiation by using four different γ-ray energies form three point sources; 356 keV from ^{133}Ba, 662 keV from ^{137}Cs as well as 1173, and 1332 keV from ^{60}Co. The γ-rays mass attenuation coefficients were plotted as a function of the doped N-HgO concentrations into N-HgO/N-Bent nanocomposites. The computed values of mass attenuation coefficients (μ_m), effective atomic number (Z_{eff}) and electron density (N_{el}) by the as-prepared samples were found to increase, while the half value layer (HVL) and mean free path (MFP) were identified to decrease upon increasing the N-HgO contents. It was concluded also that the increase in N-HgO concentration led to a direct increase in the mass attenuation coefficient from 0.10 to 0.17 cm^2/g at 356 keV and from 0.08 to 0.09 cm^2/g at 662 keV. However, a slight increase was observed in the identified mass attenuation coefficients at (1172 and 1332 keV).

1. Introduction

Ionizing radiation like gamma radiation and high energy X-rays are two of the most known dangerous radiations due to their ionizing powers and risky effects on the human tissues as well as ability to cause cancer and death [1,2]. Gamma radiation and X-rays as well as fast neutrons are produced as a result from various nuclear activities as nuclear power plants and hospital X-rays radiology rooms [3,4]. Recently nanomaterials have been introduced into a great number of nanotechnological applications including radiation shielding field [5,6]. Some nanomaterials and nanocomposites have been reported for implementation in radiation shielding of different ionizing energies. Therefore, several research papers were mainly focused on investigating of the gamma radiation shielding by using different materials including concretes, clays, polymers, and heavy metal oxides as PbO, CdO, CuO, Bi_2O_3, BaO, SrO, and others [7–28].

Tyagi et al., have reported a review article about the utilization of various kinds of industrial wastes such as cementitious materials, slags, mines wastes, polymers & glass waste, to replace the constituents of radiation shielding concretes [10]. Asal et al., have prepared ceramic bentonite clay-based materials for application in gamma radiation shielding by using different gamma rays energies from different radiation point sources (^{137}Cs, ^{251}Am, ^{57}Co, ^{60}Co, and ^{88}Y). The linear and mass attenuation coefficients of the prepared ceramics were varied from 0.479 to 1.06 cm^{-1} and from 0.238 to 0.443 cm^2/g, according to the applied thickness [11]. Agaret.al, reported a new kind of Pd-Ag alloy as gamma radiation shielding material. The mass attenuation coefficient was measured by using diverse photon energies from 81 keV to 1333 keV and the results indicated that Pd-75/Ag-25 alloy produced the maximum efficiency

* Corresponding author. Alexandria University, Faculty of Science, Chemistry Department, P.O. Box 426, Ibrahimia, 21321, Alexandria, Egypt.
E-mail address: elhassanallam@yahoo.com (E.A. Allam).

https://doi.org/10.1016/j.net.2021.12.026

towards gamma rays (about 53% at 81 keV) as well as the lowest half-value layer [12]. Nikbin et al., studied the addition of nano bismuth oxide with different percent 0, 2, 4, and 6% to heavyweight concrete and the effect of different temperatures as 25, 200, 400, and 600 °C on the gamma-ray shielding and the mechanical properties were reported. The outlined results indicated that the addition of nano bismuth oxide improved gamma rays shielding and mechanical properties at high temperatures [13]. Sayyed et al. have studied the effect of Sb_2O_3 addition as a dopant material to soda-lime glasses and the results indicated that the added Sb_2O_3 enhanced the shielding of glasses [14]. The synergistic effect of nano cadmium oxide and nano bentonite doping concentrations on polypropylene ternary nanocomposites to enhance gamma radiation shielding was also investigated and reported [15]. A newly designed glass system composed of B_2O_3-Na_2O-BaO-HgO possess effective optical and physical properties was implemented towards nuclear shielding [16] A new glass system of borate doped with mercury oxide to study its direct influence on the optical and radiation shielding properties was reported, the results indicated that the sample contains 15 wt% HgO had the highest mass attenuation coefficient, between 0.0271 and 33.4872 $cm^2\ g^{-1}$ [17]. Clays were also explored as shielding materials towards low energy photons the results indicated that photons energies below 60 keV were attenuated, however, the energies of the photons above 150 keV it was preferred doping the clay with a high Z element to increase the shielding efficiency, the clay had a density 1.99 g/cm^3 with thickness of 2 cm was found to attenuate 90% of the incident photons from Am-241s [18]. Epoxy, and its composites with Al_2O_3, and Fe_2O_3 were applied to increase the gamma radiation shielding, the results indicated that at energy 1.333 Mev epoxy alone has a mass attenuation coefficient of 0.0584 $cm^2\ g^{-1}$ and after the addition of 15% of Al_2O_3 become 0.0579 $cm^2\ g^{-1}$, and in case of Fe_2O_3 become 0.0584 $cm^2\ g^{-1}$ [19]. Mahmoud et al. tested the effects of the concentration and particle size of PbO on the mechanical and gamma-ray shielding properties of standard ceramic tiles and the results revealed that as the content of PbO (particularly PbO in nanoscale) increased, so did its mechanical performance as well as shielding capabilities [20]. Diverse composites of tungsten (VI) oxide and hydroxyethyl methacrylate-co-styrene were used and investigated to enhance thermal and radiation shielding properties [21]. Two clay materials; ball clay and kaolin were applied toward gamma radiation shielding [22]. Composites of clay and polyethylene were also studied for gamma radiation shielding [23]. Glass-based-zirconolite silicate material was investigated towards radiation shielding by using XCOM, and FLUKA simulation program [24]. In addition, other materials have been recently established and investigated as gamma radiation shielding materials [25–28].

To the best of our knowledge, focused research studies on radiation shielding properties by using composite materials including HgO nanoparticles are limited [17]. Therefore, the present study is devoted to assemble new nanocomposite (N-HgO/N-Bent) via doping different weight percentages of N-HgO (x = 10, 20, 30, and 40%) into N-Bent (100-x%) to produce a diverse percentage of the nanocomposites N-HgO/N-Bent. The as-prepared N-HgO/N-Bent systems were also aimed to characterize by FT-IR, XRD, and SEM to confirm their structural and morphological features. The efficiency and beneficiary of using N-HgO/N-Bent as effective radiation shielding nano system for γ-rays was also listed as the main targets in this study via evaluation of a number of important parameters as the mass attenuation coefficients (μm), effective atomic number (Z_{eff}), electron density (N_{el}), half value layer (HVL) and mean free path (MFP).

2. Theory

In this study, Z_{eff}, N_{el}, atomic cross sections ($\sigma_{t.a}$) and electronic cross-section ($\sigma_{t.e}$) values were obtained from Eqs. (1)–(5) by using the weight proportion (w_i), and $(\mu_m)_i$, Avogadro's number (N_A), atomic mass (N), and element fractional abundance (i) with respect to the number of the atoms (f_i) and finally, the element atomic number (Z_i) [28].

$$\mu_m = \sum_i w_i (\mu_m)_i \tag{1}$$

$$\sigma_{t.a} = \frac{\mu_m N}{N_A} \tag{2}$$

$$\sigma_{t.e} = \frac{1}{N_A} \sum \frac{f_i N_i}{Z_i} (\mu_m)_i = \frac{\sigma_{t.a}}{Z_{eff}} \tag{3}$$

$$Z_{eff} = \frac{\sigma_{t.a}}{\sigma_{t.e}} \tag{4}$$

$$N_e = \frac{\mu_m}{\sigma_{t.e}} \tag{5}$$

Where $N = \sum A_i n_i$, A_i represents the atomic weight of the element(i) and n_i represents the number of molecule formula units. On the other hand, the half values layer and the mean free path are calculated from Eqs. (6) and (7), where μ is the linear attenuation coefficient

$$HVL = \frac{ln(2)}{\mu} \tag{6}$$

$$MFP = \frac{1}{\mu} \tag{7}$$

3. Experimental details

3.1. Materials and chemicals

In this work, the employed chemicals were implemented without any purification. Sodium hydroxide (FW 40.0 g/mol, and assay >99.0%) was purchased from BDH Company, UK. Mercury chloride ($HgCl_2$, FW 271.52 g/mol and assay >99.97%) was purchased from Alpha Chemika, India. Nano bentonite ($H_2Al_2O_6Si$, FW 180.1 g/mol and assay >95.0%) was purchased from Sigma-Aldrich, USA.

3.2. Combustion synthesis of N-HgO

Synthesis of N-HgO was established in two steps. The first step included the synthesis of $Hg(OH)_2$ by mixing two solutions of $HgCl_2$ and NaOH in deionized water (25.0 mL of 0.1 mol/L NaOH solution and a 100.0 mL of 0.01 mol/L $HgCl_2$ solution). This solution was stirred at 50 °C and a yellow precipitate of mercury hydroxide was formed. This was filtrated, washed with deionized water several times to remove the excess NaOH and final $Hg(OH)_2$ product was dried at 80 °C for 4 h. The second step is related to the combustion of $Hg(OH)_2$ at 450 °C in a muffle furnace in presence of glycine based on 1:1 mass ratio and the orange N-HgO crystals product was finally formed [31,32].

3.3. Fabrication of different N-HgO/N-Bent nanosystems

N-Bent was first activated by 100 mL of 0.01 mol/L NaOH for

45 min at 80 °C and N-HgO powder was then added with different weight percentages to produce 10, 20, 30 and 40% of N-HgO/N-Bent nanosystems. All mixtures were stirred for 90 min at 90–110 °C to evaporate water content and the formed yellowish orange paste from this reaction was dried at 85 °C. Finally, the produced N-HgO/N-Bent nanosystems were ground to a fine powder.

The different N-HgO/N-Bent samples were prepared by pressing under 150 bar for 45 s using GRIMCO PRESSES under 50 tons compression press hydraulic model 50-1818-D to obtain disk with diameter = 2.6 cm, and thickness = 0.25 cm. Five different thicknesses, 0.25, 0.5, 0.75, 1.0, and 1.25 cm, were obtained by using the selected number of disks.

3.4. Characterization of the as-prepared N-HgO/N-Bent nanosystems

N-HgO, N-Bent, 10% and 40% N-HgO/N-Bent nanosystems as two selected percent concentrations of N-HgO in the nanomaterials were characterized by using diverse techniques including FT-IR, XRD and SEM as specified in Table 1.

3.5. Experimental method for mass attenuation coefficients

Using emitted 0.356, 0.662, 1.173, and 1.332 MeV gamma photons from ^{133}Ba, ^{137}Cs, and ^{60}Co point sources, the gamma-ray shielding parameters of the prepared samples were measured. The mass attenuation coefficients (μ_m) of the samples were measured by a NaI (Tl) scintillation detector (Fig. 1) with the following specification (7.5% resolution at 0.662 MeV emitted from ^{137}Cs to 0.5 mm thickness of Al window). Measurement of each sample was followed about 4 h and each measurement was repeated 3 times.

4. Results and discussions

4.1. Structural and morphological characterizations

4.1.1. FT-IR characterization

In this study, N-HgO, N-Bent, 10% and 40% N-HgO/N-Bent nanosystems were characterized by using FT-IR spectroscopy as illustrated in (Fig. 2a, b, c, and d), respectively in the range 400–4000 cm^{-1}. The investigated N-Bent (Fig. 2a) was found to exhibit the following characteristic peaks. The peak at 3631.12 cm^{-1} is referring to the stretching vibrations of the octahedral Al^{3+} cations which are coordinated with hydroxyl groups [29,30]. Three peaks at 458.11, 527.55, and 797.59 cm^{-1} are assigned to the presence of Si-O in-plane, octahedral vibrations of Al–O–Si and bending Si–O–Si. Also the peak at 797.59 cm^{-1} is due to the Al–O, and Si–O vibrations out of plane [29,30]. The broad and strong peak at 1035.81 cm^{-1} is ascribed to the silicate structure of N-Bent clay [29,30]. The two peaks at 1643.41 and 3453.73 cm^{-1} are related to the stretching and bending vibrations of the –OH groups as well as the adsorbed H_2O molecules on the surface of N-Bent [29,30] (Fig. 2b) shows the FT-IR spectrum of N-HgO and refers to the existence of two peaks at 475.47, and 588.31 cm^{-1} which are assigned to the Hg–O vibrations modes as an indication for the formation of HgO nanocrystals [31,32]. The stretching vibrations of –OH group and adsorbed water on the N-HgO surface were observed at 1464.02 and 2359.98 cm^{-1} [31,32]. On the other hand, the FT-IR spectra of as-prepared 10% and 40% N-HgO/N-Bent nanosystems are represented in (Fig. 2c and d), respectively. It is evident that they exhibited the same previously mentioned and assigned peaks in both N-HgO, and N-Bent with basic differences in their intensities according to the variation in doping percentages. However, N-Bent was found to exhibit small shifts in most characteristic peaks due possible bond formation with the doped N-HgO.

Table 1
Characterization and specifications of different techniques.

Instrument Name	Model	Data	Conditions	Technique
Fourier-transform infrared spectrophotometer	BRUKER Tensor 37	FT-IR spectrum	400–4000 cm^{-1}	Using KBr pellets
X-ray diffraction (XRD)	Shimadzu lab x 6100, Japan	The XRD pattern of the assembled composites and their components	40 kV, 30 mA, and λ = 1 Å using target Cu Kα with secondary monochromatic. 2θ = 10°–80°.	X-ray technique
Scanning electron microscope SEM	JSM-IT200, JEOL Ltd	SEM images	Imaging mode	Sputtering coating (JEOL-JFC-1100E)

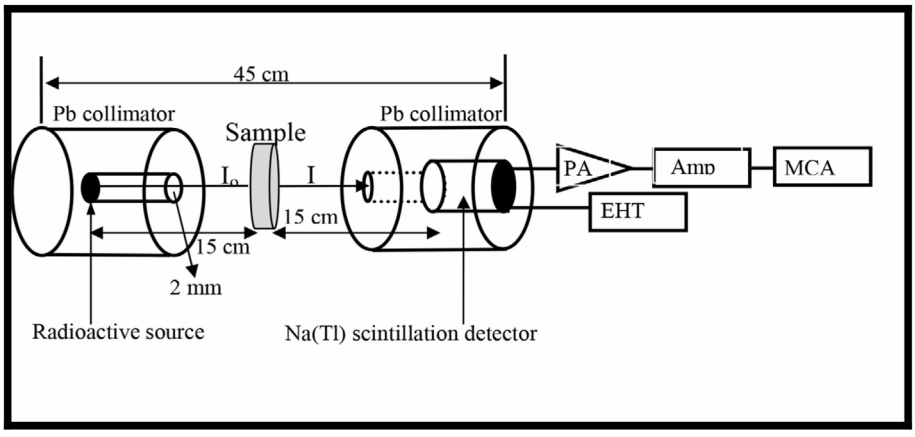

Fig. 1. Narrow beam geometrical setup consists of Pb collimator, radioactive source, NaI detector preamplifier (PA), amplifier (Amp), multi-channel analyzer (MCA) and the extra-high-tension power supply (EHT).

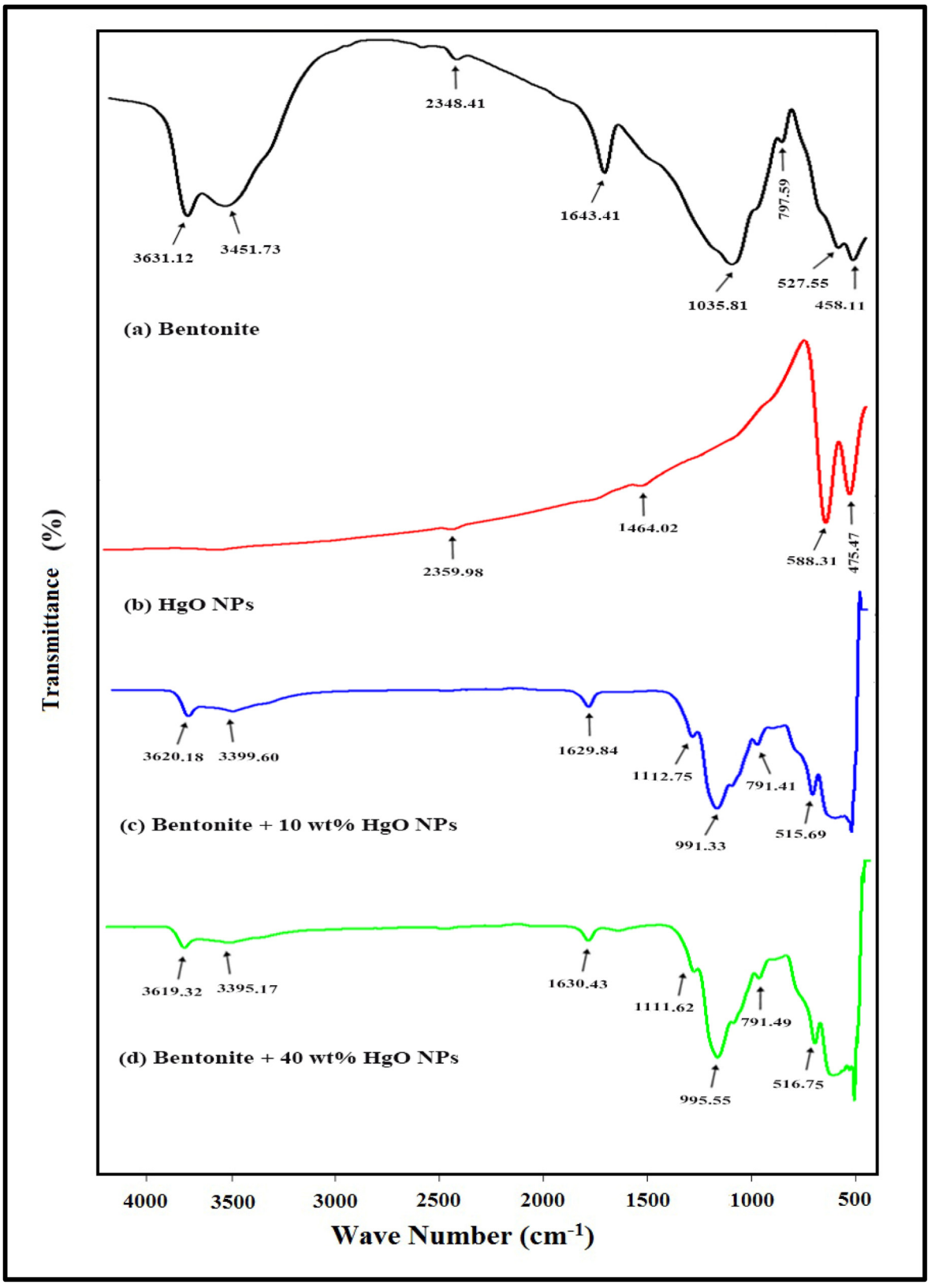

Fig. 2. FT-IR spectra of **(a)** Bentonite, **(b)** N-HgO, **(c)** Bentonite including 10% N-HgO, and **(d)** Bentonite including 40% N-HgO.

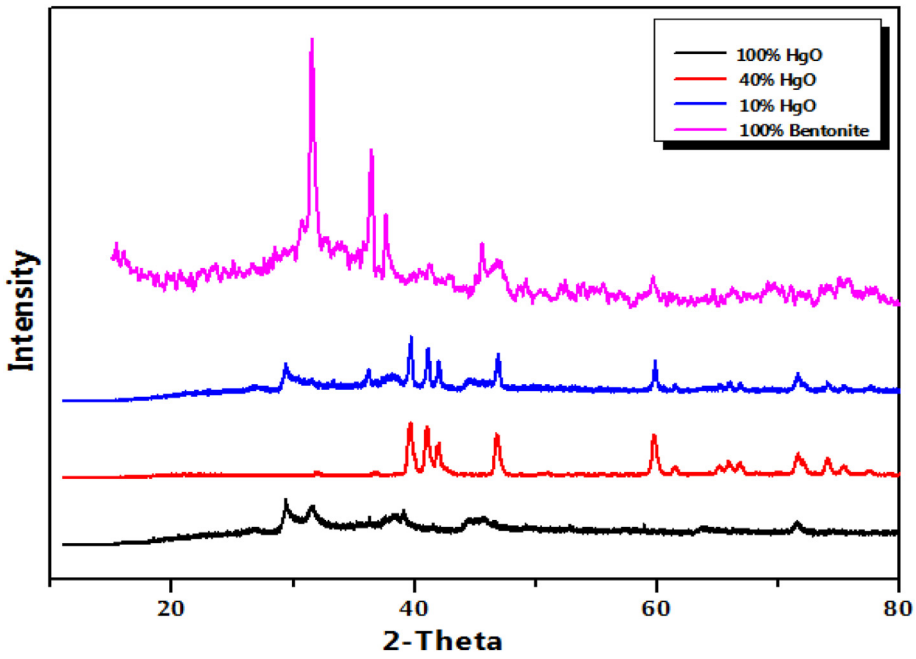

Fig. 3. XRD patterns of Bentonite, N-HgO and their corresponding nanocomposites.

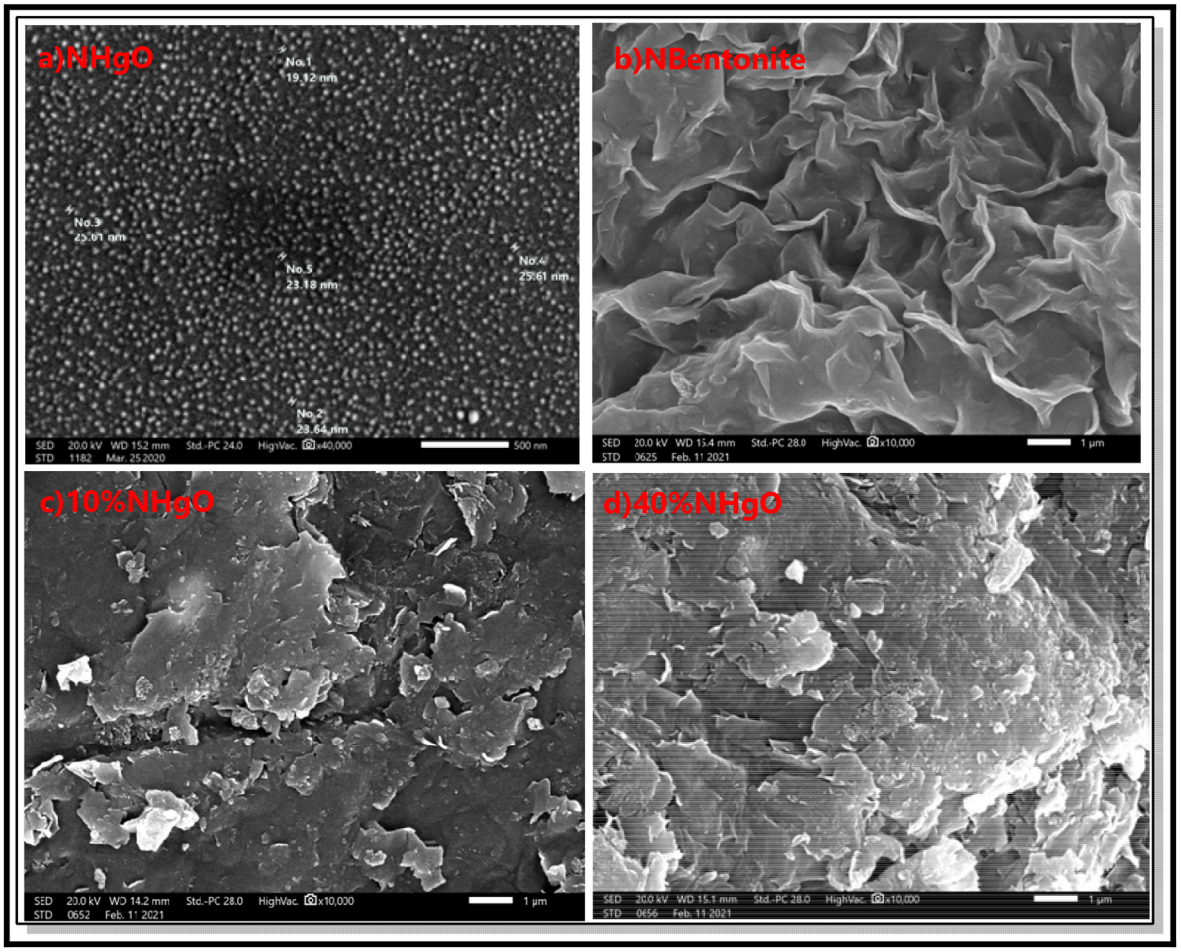

Fig. 4. SEM images of **(a)** N-HgO, **(b)** Bentonite, **(c)** Bentonite including 10% N-HgO, and **(d)** Bentonite including 40% N-HgO.

Table 2
Chemical composition by weight, thickness, density and weight fraction of elements of the prepared N-HgO/N-Bent samples.

Sample Name	Chemical Composition (wt %)		Thickness	*Density*	Weight fraction of elements					
	HgO	$Al_2H_2Na_2O_{13}Si_4$	(cm)	$g.cm^{-3}$	Hg	Al	H	Na	O	Si
1-Hg	0	100	0.25	2.447	0.0000	0.1278	0.0048	0.1089	0.4925	0.2660
2-Hg	10	90	0.25	2.664	0.0926	0.1150	0.0043	0.0980	0.4507	0.2394
3-Hg	20	80	0.25	2.976	0.1852	0.1022	0.0038	0.0871	0.4088	0.2128
4-Hg	30	70	0.25	3.239	0.2778	0.0895	0.0033	0.0762	0.3669	0.1862
5-Hg	40	60	0.25	3.647	0.3705	0.0767	0.0029	0.0653	0.3251	0.1596

Table 3
Mass attenuation coefficients of the prepared N-HgO/N-Bent samples.

Sample name	Mass Attenuation Coefficients in cm^2/g			
	356 keV	662 keV	1173 keV	1332 keV
1-Hg	0.10020	0.07663	0.05830	0.05452
2-Hg	0.11588	0.07910	0.05864	0.05461
3-Hg	0.13218	0.08221	0.05931	0.05531
4-Hg	0.14783	0.08505	0.05943	0.05518
5-Hg	0.16351	0.08799	0.05989	0.05596

4.1.2. XRD characterization

The X-ray diffraction analysis of N-Bent, N-HgO, 10% and 40% N-HgO/N-Bent nanosystems were also investigated as illustrate in (Fig. 3) The XRD pattern of N-Bent illustrates series of peaks at $2\theta = 21.0, 26.0, 27.0, 36.0, 37.0$, and 54.0°, which are corresponding to the planes (110), (210), (124), (144), (102), and (220), respectively [29,30]. These peaks provide a good evidence for the presence of aluminum silicate structure in N-Bent. Also the peaks refer and consequently confirm that the clay is composed of quartz (Q) with a trigonal structure, montmorillonite (M) with a hexagonal structure, and feldspar (F) with albite structure [29,30]. For N-HgO, the characteristic peaks were identified at $2\theta = 30.0, 31.0, 32.0, 37.0, 50.0, 51.0, 55.0, 56.0, 57.0, 61.0, 62.0, 64.0, 65.0$, and 68.0° which are attributed to the plans (011), (210), (020), (201), (221), (002), (400), (112), (230), (401), (022), (411), (420), and (302), respectively [31,32]. The XRD patterns of as-prepared10% and 40% N-HgO/N-Bent nanosystems illustrate the doping of N-HgO into N-Bent via the appearance of the previously mentioned XRD peaks for N-HgO, and N-Bent with evident difference in the peak intensity as related to the doping percentage in the nanomaterials [29–32].

4.1.3. SEM characterization

The SEM image of N-HgO refers to spherical nanoparticles as illustrated in (Fig. 4a). N-Bent was found to appear as homogenous sheets like platelets as shown in (Fig. 4b). On the other hand, the SEM images of doped N-HgO into the N-Bent layers (Fig. 4c and d) refer to be distribution of N-HgO into the N-Bent platelets by showing the spherical particles of N-HgO above the N-Bent.

4.2. Radiation shielding parameters

The prepared samples with the chemical formula (100-x%) N-Bent + x% N-HgO, where x = 0, 10, 20, 30, and 40% were studied to characterize their gamma radiation shielding properties via a number of calculated parameters. The density and weight fraction of the constituents' elements of the assembled nanocomposites are illustrated in Table 2, while Table 3 includes the μ_m values for the

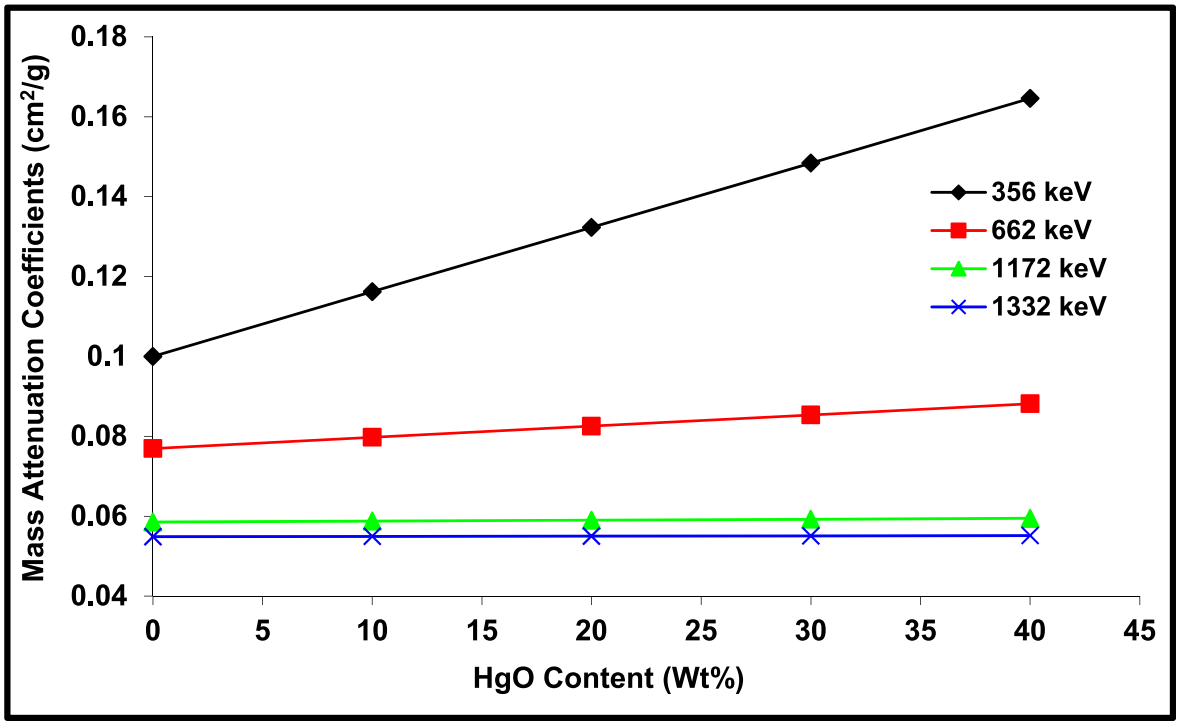

Fig. 5. Mass attenuation coefficients (μ_m) versus the wt% of N-HgO in the tested nano systems.

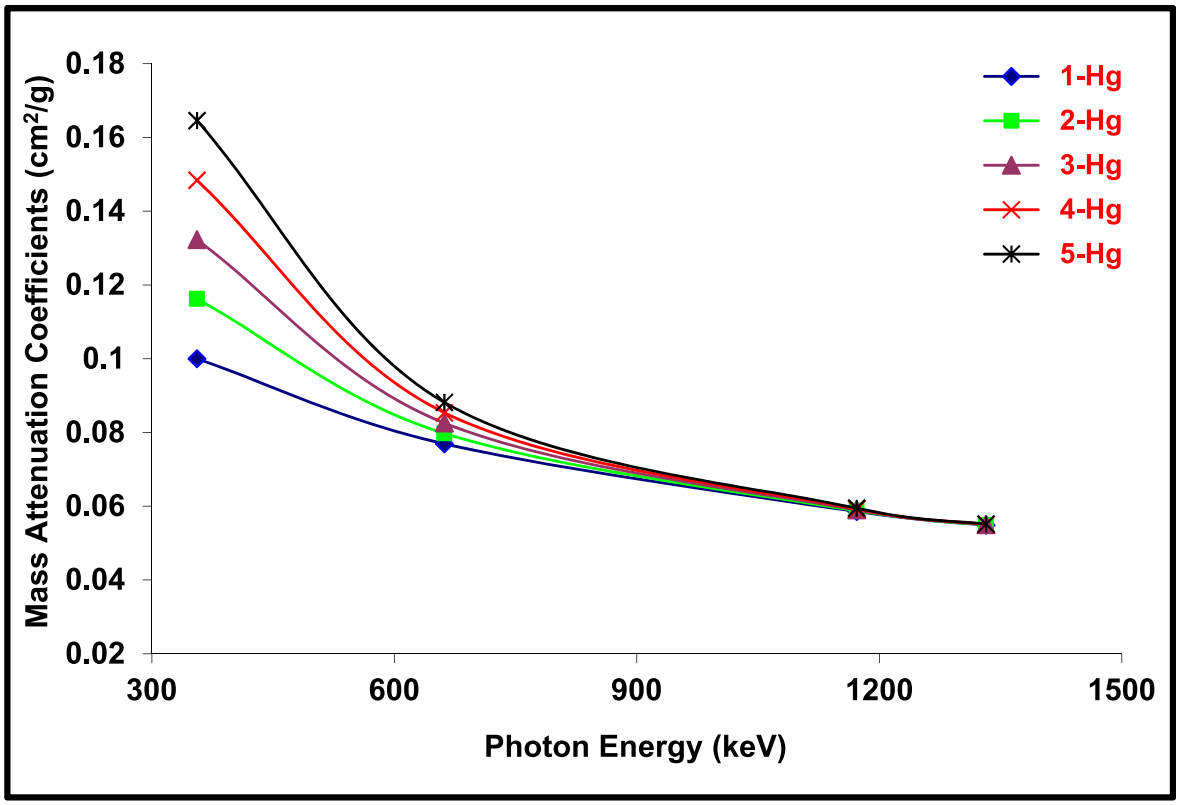

Fig. 6. Mass attenuation coefficients (μ_m) versus gamma-ray photon energy (keV).

Table 4
Effective atomic numbers of the prepared N-HgO/N-Bent samples.

Sample name	Effective Atomic Numbers (Z_{eff})			
	356 keV	662 keV	1173 keV	1332 keV
1-Hg	11.805	12.378	12.538	12.523
2-Hg	13.652	12.777	12.611	12.543
3-Hg	15.572	13.279	12.755	12.704
4-Hg	17.416	13.738	12.781	12.674
5-Hg	19.263	14.212	12.880	12.853

Table 5
Effective electron density) Nel $\times$ 10^{23}(of the prepared N-HgO/N-Bent samples.

Sample name	$N_{el} \times 10^{23}$ (electron/g)			
	356 keV	662 keV	1173 keV	1332 keV
1-Hg	2.785	2.920	2.958	2.954
2-Hg	3.220	3.014	2.975	2.959
3-Hg	3.673	3.132	3.009	2.997
4-Hg	4.108	3.241	3.015	2.990
5-Hg	4.544	3.353	3.038	3.032

investigated samples at 356, 662, 1173, and 1332 keV emitted gamma photons from ^{133}Ba,^{137}Cs, and ^{60}Co point sources (Fig. 4) shows the increase in μ_m values with increasing the percentage of N-HgO at the photon energy 356, 662, 1173, and 1332 keV. It is evident that the mass attenuation coefficients were decreased by increasing the gamma rays energies (Fig. 5). From the previous knowledge, it was reported that the mass attenuation coefficients are generally dependent on two important parameters including the sample composition, and the energy of the incident photons. The evaluated material will be more suitable for gamma radiation shielding, if it possesses a high effective mass number as a result of high number of electrons per atom. In addition, the calculated Z_{eff} values for the five investigated samples in this work have been calculated and listed in Table 4 by using the different gamma-ray photon energy in the range of 356–1332 keV. It could be concluded that the Z_{eff} values were increased by increasing the N-HgO percent. The N_{el} results of the investigated samples in the evaluated gamma-ray photon energy 356, 662, 1173, and 1332 KeV were calculated from Eq. (5) and given in Table 5. From the collected and outlined results, it was found that the N_{el} values were increased by increasing the N-HgO content in the N-Bent clay matrix. For the best radiation shielding of mixture, lower half value layer (HVL) and mean free path (MFP) values are required. So the HVL and MFP results are the most suitable quantities to describe the radiation attenuation. Table 6 shows the MFP and the HVL as a function of N-HgO content at 356, 662, 1173 and 1332 keV of gamma-ray. As expected, the MFP values were decreased with increasing N-HgO amount. Similarly, the HVL values decreased with increasing N-HgO amount. Also, it can be seen that the lowest HVL and MFP values were reported for 356 keV, whereas the highest HVL and MFP values were characterized for 1332 keV. This can be explained by the fact that the permeation abilities of gamma-rays depending on their energy (see Fig. 6).

5. Conclusion

In this study, N-HgO has been synthesized by a simple combustion method to implement this high density nanometal oxide in a new system based on doping N-HgO into N-Bent, according to the following percentage compositions (100-x%) N-Bent + x% N-HgO, where x = 0, 10, 20, 30 and 40 (weight %), the different nano-systems were prepared by the intercalation of N-HgO into the N-Bent clay layers. The diverse synthesized nanosystems were

Table 6
Half value layer (HVL) and mean free path (MFP) of the prepared N-HgO/N-Bent samples at different gamma ray photon energies.

Sample	356 keV		662 keV		1173 keV		1332 keV	
	HVL(cm)	MFP(cm)	HVL(cm)	MFP(cm)	HVL(cm)	MFP(cm)	HVL(cm)	MFP(cm)
1-Hg	2.8264	4.0785	3.6957	5.3329	4.8577	7.0097	5.1945	7.4957
2-Hg	2.2449	3.2393	3.2887	4.7456	4.4361	6.4014	4.7635	6.8737
3-Hg	1.7617	2.5422	2.8325	4.0874	3.9262	5.6655	4.2101	6.0752
4-Hg	1.4473	2.0885	2.5156	3.6301	3.6001	5.1950	3.8774	5.5951
5-Hg	1.1621	1.6769	2.1596	3.1162	3.1728	4.5784	3.3956	4.8999

characterized by using FT-IR, XRD and SEM and implemented towards effective gamma radiation shielding by using diverse gamma-ray photon energies (356, 662, 1173 and 1332 keV). The study of shielding parameters by the as-prepared nanosystems referred to the high incorporated shielding properties for γ-rays based on the computed μ_m, Z_{eff}, electron density (N_{el}), half-value layer (HVL), and mean free path (MFP). The identified μ_m, Z_{eff}, and N_{el} values of the investigated samples at the selected gamma-ray photon energies were increased with increasing the N-HgO percentage. On the other hand, the half-value layer (HVL) and mean free path (MFP) results were decreased upon increasing the N-HgO content. Consequently, the present study provided excellent nanosystems for application in gamma-rays shielding with the aim of minimization of the deleterious effects of radiation [33].

Declaration of competing interest

The authors declare that they have no known competing financial interests or personal relationships that could have appeared to influence the work reported in this paper.

Acknowledgment

The authors extend their appreciation to the Deanship of Scientific Research at King Khalid University for funding this work through Research Groups Project under grant number (R.G.P1./229/1442).

References

[1] O. Baykara, S.G. Irim, A.A. Wis, M.A. Keskin, G. Ozkoc, A. Avcı, M. Dorgu, Polyimide nanocomposites in ternary structure: “A novel simultaneous neutron and gamma-ray shielding material”, Polym. Adv. Technol. 31 (2020) 2466–2479.
[2] F. Akman, Z.Y. Khattari, M.R. Kaçal, M.I. Sayyed, F. Afaneh, The radiation shielding features for some silicide, boride and oxide types ceramic, Radiat. Phys. Chem. 160 (2019) 9–14.
[3] D.K. Gaikwad, M.I. Sayyed, S.S. Obaid, S.A.M. Issa, P.P. Pawar, Gamma ray shielding properties of TeO_2-ZnF_2-As_2O_3-Sm_2O_3 glasses, J. Alloys Compd. 765 (2018) 451–458.
[4] A.S. Wagha, S.Y. Sayenko, A.N. Dovbnya, V.A. Shkuropatenko, R.V. Tarasov, A.V. Rybka, A.A. Zakharchenko, Durability and shielding performance of borated Ceramicrete coatings in beta and gamma radiation fields, J. Nucl. Mater. 462 (2015) 165–172.
[5] A.M.A. Mostafa, A.M. Shams, M.I. Sayyed, Gamma ray shielding properties of PbO-B_2O_3-P_2O_5 doped with WO_3, J. Alloys Compd. 708 (2017) 294–300.
[6] H.O. Tekin, M.I. Sayyed, Shams A.M. Issa, Gamma radiation shielding properties of the hematite-serpentine concrete blended with WO_3 and Bi_2O_3 micro and nano particles using MCNPX code, Radiat. Phys. Chem. 150 (2018) 95–100.
[7] C. Bootjomchai, J. Laopaiboon, C. Yenchai, R. Laopaiboon, Gamma-ray shielding and structural properties of barium–bismuth–borosilicate glasses, Radiat. Phys. Chem. 81 (2012) 785–790.
[8] S. Tuscharoen, J. Kaewkhao, P. Limkitjaroenporn, P. Limsuwan, W. Chewpraditkul, Improvement of BaO: B_2O_3:Fly ash glasses: radiation shielding, physical and optical properties, Ann. Nucl. Energy 49 (2012) 109–113.
[9] R.M. El-Sharkawy, K.S. Shaaban, R. Elsaman, E.A. Allam, A. El-Taher, M.E. Mahmoud, Investigation of mechanical and radiation shielding characteristics of novel glass systems with the composition xNiO–20ZnO–60B_2O_3–(20-x) CdO based nanometal oxides, J. Non-Cryst. Solids 528 (2020), 119754.
[10] G. Tyagi, A. Singhal, S. Routroy, D. Bhunia, M. Lahoti, A review on sustainable utilization of industrial wastes in radiation shielding concrete, Mater. Today Proc. 32 (2020) 746–751 ().
[11] S. Asal, S.A. Erenturk, S. Haciyakupoglu, Bentonite based ceramic materials from a perspective of gamma-ray shielding: preparation, characterization and performance evaluation, Nucl. Eng. Technol.1634–1641 (2021) 535 .
[12] O. Agar, M.I. Sayyed, F. Akman, H.O. Tekin, M. R Kaçal, An extensive investigation on gamma ray shielding features of Pd/Ag-based alloys, Nucl. Eng. Technol.) 853–859 (2019) 51).
[13] I.M. Nikbin, A. Rafiee, S. Dezhampanah, S. Mehdipour, R. Mohebbi, H. H Moghadam, A. Sadrmomtazi, Effect of high temperature on the radiation shielding properties of cementitious composites containing nano-Bi_2O_3, J. Mater. Res. Technol. 9 (2020) 11135–11153 ().
[14] M.I. Sayyed, K.A. Mahmoud, O.L. Tashlykov, M. U Khandaker, M.R. I Faruque, Enhancement of the shielding capability of soda–lime glasses with Sb_2O_3 dopant: a potential material for radiation safety in nuclear installations, Appl. Sci. 11 (2021) 326. .
[15] R.M. El-Sharkawy, E.A. Allam, A. El-Taher, E.R. Shaaban, M.E. Mahmoud, Synergistic effect of nano-bentonite and nano cadmium oxide doping concentrations on assembly, characterization, and enhanced gamma-rays shielding properties of polypropylene ternary nanocomposites, Int. J. Energy Res. 45 (2021) 8942–8959.
[16] A.S. Abouhaswa, E. Kavaz, A novel B_2O_3-Na_2O-BaO-HgO glass system: synthesis, physical, optical and nuclear shielding features, Ceram. Int. 46 (2020) 16166–16177 ().
[17] A.S. Abouhaswa, M.I. Sayyed, K.A. Mahmoud, Y. Al-Hadeethi, Direct influence of mercury oxide on structural, optical and radiation shielding properties of a new borate glass system, Ceram. Int. 46 (2020) 17978–17986 ().
[18] S.M. Tajudin, A.H.A. Sabri, M.Z.A. Aziz, S.F. Olukotun, B.M. Ojo, M.K. Fasasi, Feasibility of clay-shielding material for low-energy photons (Gamma/X), Nucl. Eng. Technol. 51 (2019) 1633–1637.
[19] M.J. Aldhuhaibat, M.S. Amana, N.J. Jubier, A.A. Salim, Improved gamma radiation shielding traits of epoxy composites: evaluation of mass attenuation coefficient, effective atomic and electron number, Radiat, Phys. Chem. 179 (2021), 109183 ().
[20] M.E. Mahmoud, A.M. El-Khatib, A.M. Halbas, R.M. El-Sharkawy, Ceramic tiles doped with lead oxide nanoparticles: their fabrication, physical, mechanical characteristics and γ-ray shielding performance, Radiat. Phys. Chem. 189 (2021), 109780.
[21] B. Körpınar, B.C. Öztürk, N.F. Çam, H. Akat, Investigations on thermal and radiation shielding properties of the poly (hydroxy ethyl methacrylate-co-styrene)/tungsten (VI) oxide composites, Prog.Nucl.Energy 126 (2020), 103424 ().
[22] S.F. Olukotun, S.T. Gbenu, F.I. Ibitoye, O.F. Oladejo, H.O. Shittu, M.K. Fasasi, F.A. Balogun, Investigation of gamma radiation shielding capability of two clay materials, Nucl. Eng. Technol. 50 (2018) 957–962. .
[23] S.F. Olukotun, S.T. Gbenu, O.F. Oladejo, M.I. Sayyed, S.M. Tajudin, O.G. Fadodun, A.A. Amosun, M.K. Fasasi, Investigation of gamma ray shielding capability of fabricated clay-polyethylene composites using EGS5, XCOM and Phy-X/PSD, Radiat. Phys. Chem. 177 (2020), 109079 ().
[24] H. Akyildirim, E. Kavaz, F.I. El-Agawany, E. Yousef, Y.S. Rammah, Radiation shielding features of zirconolite silicate glasses using XCOM and FLUKA simulation code, J. Non-Cryst. Solids 545 (2020), 120245 ().
[25] A. Temir, K.S. Zhumadilov, M.V. Zdorovets, I.V. Korolkov, A. Kozlovskiy, A.V. Trukhanov, Synthesis, phase transformations, optical properties and efficiency of gamma radiation shielding by Bi_2O_3-TeO_2-WO_3 ceramics, Opt. Mater. 113 (2021), 110846 ().
[26] I. Ebrahimi, M.P. Gashti, Chemically reduced versus photo-reduced clay-Ag-polypyrrole ternary nanocomposites: comparing thermal, optical, electrical and electromagnetic shielding properties, Mater. Res. Bull. 83 (2016) 96–107. .
[27] S. Akbulut, A. Sehhatigdiri, H. Eroglu, S. Çelik, A research on the radiation shielding effects of clay, silica fume and cement samples, Radiat. Phys. Chem. 117 (2015) 88–92. .
[28] M.E. Mahmoud, R.M. El-Sharkawy, E.A. Allam, Reda Elsaman, Atef El-Taher, Fabrication and characterization of phosphotungstic acid - copper oxide nanoparticles - plastic waste nanocomposites for enhanced radiation-

shielding, J. Alloys Compd. 803 (2019) 768–777.
[29] M.E. Mahmoud, E.A. Allam, E.A. Saad, A.M. El-Khatib, M.A. Soliman, Remediation of Co/Zn ions and their ^{60}Co/^{65}Znradioactive nuclides from aqueous solutions by acid activated nanobentonite, Environ. Nanotechnol. Monit. Manag. 12 (2019), 100277.
[30] M.E. Mahmoud, E.A. Allam, E.A. Saad, A.M. El-Khatib, M.A. Soliman, Intercalation of nanopolyaniline with nanobentonite and manganese oxide nanoparticles as a novel nanocomposite to remediate cobalt/zinc and their radioactive nuclides ^{60}Co/^{65} Zn, J. Polym. Environ. 27 (2019) 421–433 ().
[31] E.A. Abdelrahman, R.M. Hegazey, Facile synthesis of HgO nanoparticles using hydrothermal method for efficient photocatalytic degradation of crystal violet dye under UV and sunlight irradiation, J. Inorg. Organomet. Polym. 29 (2019) 346–358 ().
[32] A. Askarinejad, A. Morsali, Synthesis and characterization of mercury oxide unusual nanostructures by ultrasonic method, Chem. Eng. J. 153 (2009) 183–186 ().
[33] H.M.H. Zakaly, A. Ashry, A. El-Taher, A.G.E. Abbady, E.A. Allam, R.M. El-Sharkawy, M.E. Mahmoud, Role of novel ternary nanocomposites polypropylene in nuclear radiation attenuation properties: in-depth simulation study, Radiat. Phys. Chem. 188 (2021), 109667.